Uttam Kumar Mohanty
Department of Mechanical and Aerospace Engineering,
Indian Institute of Technology Hyderabad,
Sangareddy 502285, India
e-mail: me15resch11004@iith.ac.in

Yohei Abe
Technical Research Institute,
Hitachi Zosen Corporation,
Osaka 551-0022, Japan
e-mail: y_abe@hitachizosen.co.jp

Takahiro Fujimoto
Technical Research Institute,
Hitachi Zosen Corporation,
Osaka 551-0022, Japan
e-mail: ta_fujimoto@hitachizosen.co.jp

Mitsuyoshi Nakatani
Technical Research Institute,
Hitachi Zosen Corporation,
Osaka 551-0022, Japan
e-mail: nakatani_m@hitachizosen.co.jp

Akikazu Kitagawa
Technical Research Institute,
Hitachi Zosen Corporation,
Osaka 551-0022, Japan
e-mail: kitagawa_a@hitachizosen.co.jp

Manabu Tanaka
Joining and Welding Research Institute,
Osaka University,
Osaka 567-0047, Japan
e-mail: tanaka@jwri.osaka-u.ac.jp

Tetsuo Suga
Joining and Welding Research Institute,
Osaka University,
Osaka 567-0047, Japan
e-mail: suga@jwri.osaka-u.ac.jp

Abhay Sharma[1]
Department of Materials Engineering,
Faculty of Engineering Technology,
KU Leuven,
Campus De Nayer, Sint-Katelijne-Waver 2860,
Belgium
e-mail: abhay.sharma@kuleuven.be

Performance Evaluation of Alternating Current Square Waveform Submerged Arc Welding as a Candidate for Fabrication of Thick Welds in 2.25Cr-1Mo Heat-Resistant Steel

The paper evaluates the performance of alternating current (AC) square waveform submerged arc welding (SAW) as a candidate technology for manufacturing thick welds for high-pressure vessels. A new mathematical formulation for calculating melting efficiency in square waveform arc welding is presented. The melting efficiency and the heat consumption are presented as a mathematical model of welding parameters, namely welding current, welding speed, current frequency, and electrode negativity (EN) ratio. The proposed approach is demonstrated through the welding of 2.25Cr-1Mo heat-resistant steel performed over a wide range of welding parameters. The investigation provides deeper insights into the interplay between process parameter, total heat consumption, and melting efficiency. The effect on flux consumption is also explained. The melting efficiency is inversely proportional to flux consumption. The welding heat does not necessarily promote the plate melting. Improper use of welding heat may lead to decreased melting efficiency and increased unwanted melting and consumption of welding flux. Compared to the conventional direct current (DC) power sources, the AC square waveform welding achieves almost the same order of melting efficiency with added advantages of better weld bead shape and flux consumption in a desirable range. The two additional parameters (frequency and EN ratio) of the AC square waveform power source provide more freedom to fine-tune the process and thereby efficiently use welding heat. The results of this investigation will be advantageous to the designers and fabricators of high-pressure vessels using AC square waveform welding. [DOI: 10.1115/1.4046785]

Keywords: submerged arc welding, heat-resistant steel, melting efficiency, bead geometry, flux-to-wire-ratio

1 Introduction

The ever-increasing demand for energy—obtained through natural (oil and natural gas) or human-made sources (thermal, nuclear, etc.)—requires the manufacture of high-quality pressure vessels and pipeline networks. The heavy fabrication industry extensively uses submerged arc welding (SAW) to manufacture pressure vessels and pipelines because of SAW's clean, energy-efficient operation without welding fumes, and excellent surface appearance. Several efforts have been made, from different directions, to improve the quality of thick weld joints used in pressure vessels and pipes, e.g., improving the mechanical properties [1], fracture resistance [2], etc. Simultaneously, new welding processes or their variants are being introduced for better productivity, e.g., multiple-wire SAW [3].

The SAW is known for its highest arc efficiency (i.e., the proportion of electric power used in heating and melting) among the arc welding processes. The melting is a combined result of arc-heating and joule-heating. The arc-heat is associated with the

[1]Corresponding author.

Contributed by the Pressure Vessel and Piping Division of ASME for publication in the Journal of Pressure Vessel Technology. Manuscript received September 30, 2018; final manuscript received February 19, 2020; published online April 16, 2020. Assoc. Editor: Bostjan Bezensek.

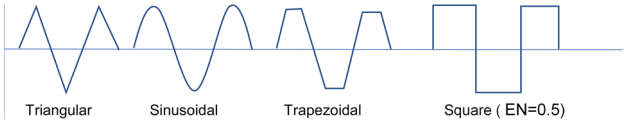

Fig. 1 Waveforms used in arc welding

emission of electrons. A considerable amount of voltage is utilized in electrons' origination at the cathode tip that is surrounded by a sheath of positive ions. The voltage gradient, therefore, is more near the cathode (compared to the anode) that facilitates enhanced heating and melting at the cathode. The electrons, which constitute a major proportion of welding current, emit from the cathode. Therefore, the current density at the cathode is higher compared to the anode. The higher current density is directly related to enhanced joule-heating. When the electrode is at the cathode, the current density further increases so as to improve the joule-heating and electrode-melting rate. The combined effect of arc and joule-heating on electrode (i.e., wire) melting rate is expressed as follows:

$$\mathrm{MR} = a_1 I + a_2 \frac{I^2 L}{d^2} \tag{1}$$

where I is the welding current, L is the electrode extension, and d is the wire diameter. The coefficients a_1 and a_2 signify the proportion of arc and joule-heating, respectively. The values of these coefficients are higher for direct current electrode negative (DCEN) polarity because of the reasons explained previously [4]. On the other hand, because of the same reasons, direct current electrode positive (DCEP) polarity results in enhanced plate melting and deeper weld penetration. The DCEP also results in the removal of oxides from the weld pool (cleaning action) because of the bombardment of heavy positive ions on the negative weld plate. The alternating current (AC) inherits benefit of positive and negative polarities, particularly for welding of light materials like aluminum. However, the arc extinguishes every half cycle at the crossover (polarity reversal) that leads to a kind of arc instability that becomes more critical in SAW that operates at higher voltage and currents.

A square AC waveform provides instantaneous polarity reversal without extinguishing the welding arc. The arc remains stable, and an excellent bead appearance is obtained with reduced distortion [5]. Toma et al. [6] recommended the AC square waveform over DCEP for better toughness in low-temperature environments. The practical advantages of the AC square waveform encouraged scientific studies using advanced tools, like three-dimensional computational fluid dynamics simulations [7], semi-analytical nonlinear models for weld profile prediction [8], and high-speed videography of metal transfer [9]. The higher heating while a negative electrode increases the melting rate that results in a higher frequency of metal droplet detachment. The AC square waveform can maintain penetration at higher welding speeds [8]. In combination with DCEP (at the lead wire), the trailing electrode with the AC square waveform in tandem welding enhances the deposition rate [10]. Despite these developments, many more investigations are required to fully understand the capabilities of the square waveform process in terms of its melting efficiencies, particularly for materials like 2.25Cr-1Mo heat-resistant steel that is used for pressure vessels, petroleum and chemical plants due to its excellent mechanical properties at elevated temperatures.

The review indicates the significance of melting efficiency. The progress on the predictability of melting efficiency of weld plate and electrode over a wide range of process parameters is limited. Fabrication of highly efficient welded products of special materials using new processes (e.g., the focus of the present investigation—AC square wave SAW of heat-resistant steel for pressure vessels) requires researchers to develop a systematic approach for predicting melting efficiency. Owing to the same, the present investigation is broadly aimed at a mathematical-cum-statistical formulation for prediction of electrode and plate melting efficiencies as functions of welding process parameters. A mathematical formulation for computing melting efficiencies is presented that uses experimentally measured current, voltage, and bead cross-sectional area as inputs. As the heat input and area of cross section are functions of the process parameters, the computed melting efficiencies are presented as a predictive model of shop-floor-controlled process parameters. The specific aim of this investigation is to comprehend the effect of process parameters on the melting efficiency of AC square waveform SAW for a candidate material, 2.25Cr-1Mo heat-resistant steel, and evaluate the interplay between the process parameters, melting efficiencies, and resulting effects (e.g., deposition rate and flux consumption rate).

2 Materials and Experiments

The AC square waveform welding power source is one of the latest additions in the series of power sources for submerged arc welding. The AC in triangular, sinusoidal, trapezoidal, etc. forms, as shown in Fig. 1, has been successfully used in other arc welding processes, like gas metal arc welding (GMAW) and gas tungsten arc welding (GTAW), for many decades. The same waveforms are not appropriate for SAW because of the lowering of the voltage while changing over polarity extinguishes the arc. With an electronically controlled power source, the instantaneous changeover of polarity maintains a high-enough voltage to avoid extinguishing the arc. The proportion of a time-cycle for which an electrode remains negative is known as electrode negativity ratio (EN ratio).

The AC square wave SAW experiments were conducted at Hitachi-Zosen Corporation, Japan, with an experimental setup shown in Fig. 2. ASTM A387 Grade 22 steel (600 mm

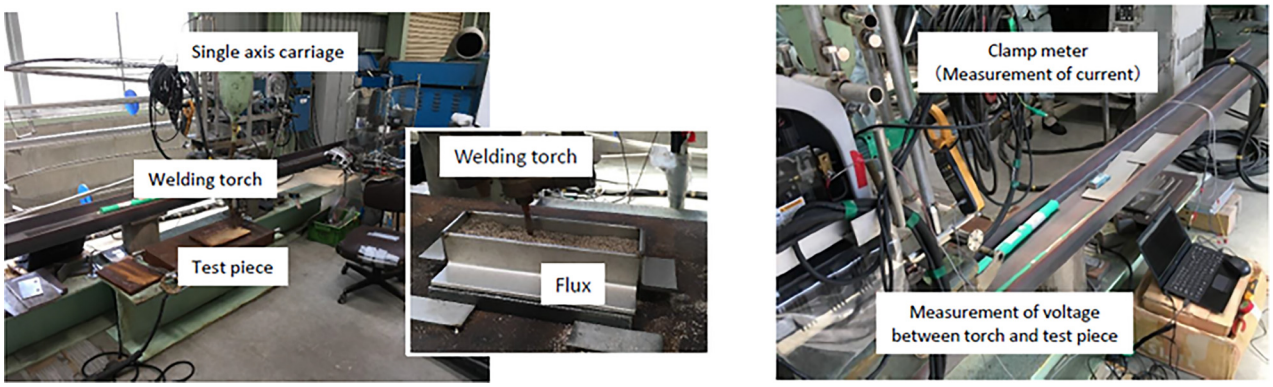

Fig. 2 Experimental setup of the AC square waveform SAW

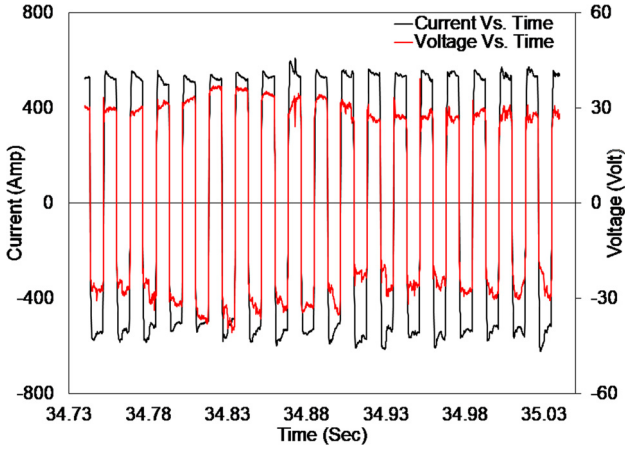

Fig. 3 Actual current and voltage signals

$\times$ 80 mm $\times$ 20 mm) was a workpiece material, a 4-mm-diameter US-521S wire was used as an electrode, and PF-200 was flux material used for the experiment, supplied by Kobelco, Hyogo, Japan. The dynamic welding current and voltage signals were recorded using a current sensor and data acquisition system. The variations of the current and voltage signals are shown in Fig. 3.

The experiments were conducted using an L16 orthogonal array with varying frequency, EN ratio, current, and welding speed values, as shown in Table 1. Additionally, ten experiments were conducted to make the calculation robust. The experimental observations were randomly divided into two groups: model development and model validation. The welding voltage (30 V) and contact-tip-to-workpiece-distance (25 mm) were kept constant. Two experiments were conducted under DCEN and DCEP conditions (i.e., EN = 1 and EN = 0, respectively) to calibrate the

Table 1 Experimental conditions

	Frequency (Hz)	EN ratio	Current (A)	Welding speed (cm/min)
Model development	60	0.5	500	30
	60	0.5	400	30
	60	0.5	600	30
	60	0.5	500	20
	60	0.5	500	50
	60	0.75	500	30
	20	0.5	500	30
	80	0.5	500	30
	20	0.25	500	20
	40	0.4	500	40
	80	0.75	500	50
	40	0.25	700	30
	80	0.5	700	20
	60	0.75	700	40
	20	0.4	700	50
	80	0.4	400	30
	60	0.25	400	50
	20	0.75	600	30
	60	0.4	600	20
	80	0.25	600	40
	40	0.5	600	50
Validation	60	0.5	700	30
	60	0.5	500	40
	60	0.4	500	30
	60	0.25	500	30
	40	0.5	500	30
DC	DCEP	0	500	30
	DCEN	1	500	30

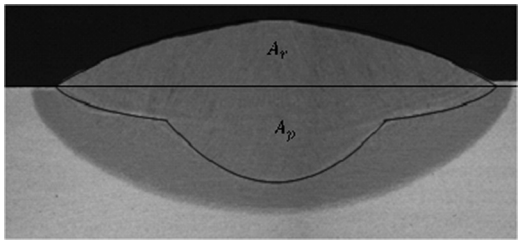

Fig. 4 Sample macrograph for calculating penetration area and reinforcement area

polarity effect on weld metal temperature, as discussed later in this article.

To get the desirable weld features, the weld-bead cross section was cut using a wire electrical discharge machining perpendicular to the welding direction, and then samples were ground and polished mechanically with emery papers of varying grit sizes (from 200 to 2000). After that, the samples were etched with 5% nital solution and macrographs were obtained, as shown in Fig. 4. The penetration area and reinforcement area of weld-bead were measured from the macrographs using IMAGE J software.

3 Mathematical Formulation for Calculation of Melting Efficiency

3.1 Background. The melting is a fundamental characteristic in arc welding, which involves melting of base metal and electrode. The efficient use of heat generated by an electric arc under a given set of welding conditions directly affects the quality and productivity of resulting weld. The total arc energy (E_{Total}), as shown in Fig. 5(*a*), can be expressed as the sum of energy supplied to the fusion zone ($E_{\text{Fusion Zone}}$), workpiece ($E_{\text{Workpiece}}$), and energy lost (E_{Loss}) to the surroundings due to conduction, convection, and radiation (i.e., $E_{\text{Total}} = E_{\text{Fusion Zone}} + E_{\text{Workpiece}} + E_{\text{Loss}}$). A complete understanding of melting behavior shows that total energy generated by an electric arc is not fully utilized for melting of workpiece and electrode material. The fraction of energy utilized to melt an electrode is termed as electrode melting efficiency (η_e), whereas remaining proportion, which is used to melt workpiece, is known as plate melting efficiency (η_p). The regions of the fusion zone, namely penetration area (A_{p}) and reinforcement area (A_{r}) (Fig. 5(*b*)), are good measurers of η_e and η_p, respectively.

The total melting efficiency (i.e., the sum of melting efficiencies ($\eta_m = \eta_e + \eta_p$) cannot be 100% because of losses; however, they may be altered because of material and its dimensions (thick or thin), sets of welding conditions, and mechanism of the welding process. A proper selection of process parameters may enhance individual and total melting efficiencies. The melting efficiency is influenced by the welding process and its variants. Su et al. [11] observed that AC double pulse GMAW is more efficient than DC pulsed GMAW because of higher wire melting efficiency and better control of the molten pool profile. Kah et al. [12] observed that melting efficiency values of arc leading hybrid, laser leading hybrid, autogenous laser, backhand arc, and forehand arc welding increase in ascending order. Bajcer et al. [13] observed a significant difference between single-wire and multiple-wire welding and observed that the melting efficiency of multiple-wire welding is more than that of single-wire welding. Unocic and DuPont [14] studied the effect of laser power, welding speed, and powder mass flowrate on melting efficiency in a laser engineered net shaping process. Shen et al. [15] compared electrode melting efficiency and plate melting efficiency of single- and multiple-wire SAW and related them with heat input. The electrode melting efficiency increases and decreases with increases in heat input in single- and multiple-wire SAW, respectively, whereas no significant variation in plate melting efficiency was observed.

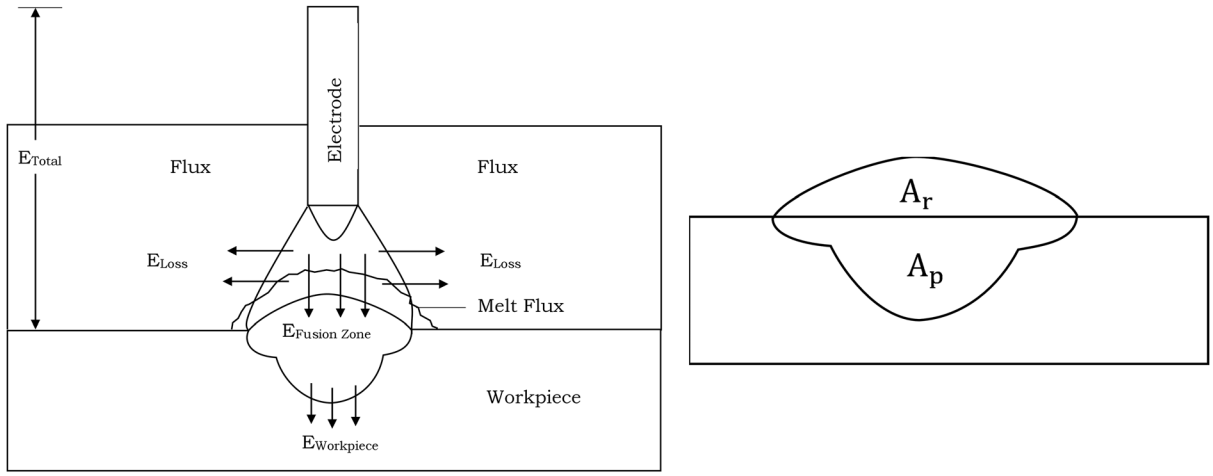

(*a*) (*b*)

Fig. 5 (*a*) Energy distribution in arc welding and (*b*) quantitative representation of weld bead

The melting efficiency is sensitive to the quality of consumable and secondary aspects, like the geometry of the weld plate. The flux in activated GTAW improves melting efficiency because of improvements in electromagnetic force and arc pressure, which improve fluid flow [16]. The combination of various fluxes in flux-cored arc welding, in comparison with the individual flux-rich environment, enhances the molten metal volume [17]. Tusek and Suban [18] reported that increased hydrogen content in shielding gas increases melting efficiency. Increases in electrode wire diameter have a negative impact on melting efficiency [19].

Few reported investigations have quantified melting efficiency. Zhu et al. [20] developed a melting efficiency expression in terms of melting energy of fusion zone and total energy transferred to workpiece in GMAW. Walsh et al. [21] developed an empirical relation of melting efficiency using cross-sectional area of fusion zone, welding speed, laser output power, and change in enthalpy of a high-power diode-laser. Lee et al. [22] related melting efficiency with measured bead area and welding parameters in SAW. Achebo and Oghoore [23] obtained melting efficiency using an exponential function of the laser power of CO_2 laser welding process. A comprehensive formulation for the prediction of melting efficiency in terms of process parameters, which is yet not developed, is presented in this article.

3.2 Mathematical Formulation. The plate and electrode melting efficiency can be calculated with the help of penetration and reinforcement area of a weld bead, respectively. These efficiencies are functions of fusion areas (A_P and A_r) and theoretical cross-sectional area (A_{th}) as follows:

$$\eta_p = \frac{A_p}{A_{\text{th}}} \times 100 \tag{2}$$

$$\eta_e = \frac{A_r}{A_{\text{th}}} \times 100 \tag{3}$$

The theoretical cross-sectional area is calculated from actual heat input (H_a) by using the following relation [24]:

$$A_{\text{th}} = \frac{\hat{v}}{q_{\text{eq}}} \times H_a,\ \text{mm}^2 \tag{4}$$

where $\hat{v}$ is the specific volume of weld metal in mm^3/g, q_{eq} is the heat required to melt a unit mass of metal, and H_a is the heat input per unit length in J/mm.

The heat required to melt weld metal can be expressed in generic form as

$$q = \Delta H_{T_m} + \int_{T_m}^{T\max} C_p dT \tag{5}$$

where $\Delta H_{T_m} = (H_{T_m} - H_{T_a})$ is the enthalpy difference between the melting point temperature and ambient temperature. For a constant pressure heating process, the expression $\int_{T_m}^{T\max} C_p dT$ becomes $(H_{T_{\max}} - H_{T_m})$. Therefore, the heat required to melt weld metal expression may be written as

$$q = (H_{T_m} - H_{T_a}) + (H_{T_{\max}} - H_{T_m}) = (H_{T_{\max}} - H_{T_a}),\ \text{J} \tag{6}$$

The heat required to melt weld metal is calculated by using enthalpy–temperature relation, as shown in Fig. 6, obtained from THERMO-CALC 2017A software. Since weld metal is an alloy, it consists of different periodic elements, different atomic masses with different proportions, as shown in Table 2. The molecular weight can be obtained via a combined molecular weight of each element to calculate an equivalent heat required to melt weld metal. The generic expression for equivalent molecular weight and heat required to melt weld metal can be expressed as

$$M_{\text{eq}} = \left(\frac{\sum p_i \times A_i}{\sum p_i}\right),\ \text{g} \tag{7}$$

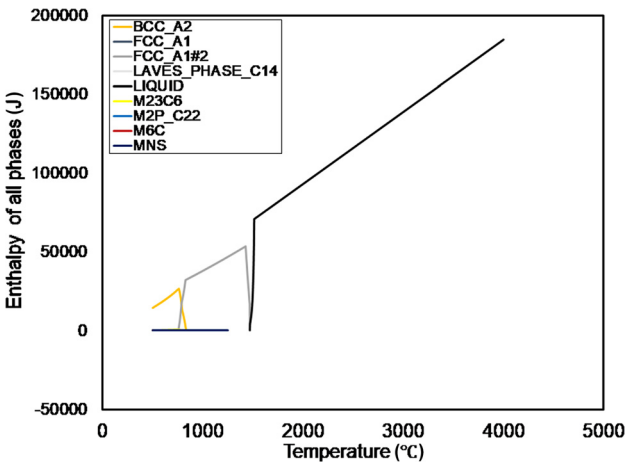

Fig. 6 Enthalpy of all phases

Table 2 Elemental composition and atomic mass of a weld metal

Weld metal	C	Si	Mn	P	S	Ni	Cr	Mo	Cu	Fe
Composition (p_i)	0.12	0.1	0.82	0.008	0.001	0.13	2.34	1.04	0.12	95.321
Atomic mass (A_i)	12.01	28.1	54.94	30.97	32.06	58.69	51.99	95.94	63.55	55.84

$$q_{\text{eq}} = \left(\frac{q}{M_{\text{eq}}}\right), \text{J/g} \tag{8}$$

where p_i and A_i are the percentage contribution and atomic mass of the element and M_{eq} and q_{eq} are equivalent molecular weight and heat required to melt weld metal, respectively.

The maximum temperature of molten metal is difficult to know as the weld pool does not have a uniform temperature. Perhaps the literature, therefore, lacks consistency in maximum temperature, e.g., Niles and Jackson [25] set 1750 °C as the maximum effective temperature to calculate the heat content of mild steel using the GTAW process, whereas the actual maximum temperature lies in between 2000 and 2300 °C. Similarly, King [26] assumed that the maximum temperature lies in a range of 3000–4000 °C for 2.25Cr-1Mo steel weld metal, which is too wide to be used in melting efficiency computation. Moreover, the weld pool has a temperature variation vis-à-vis a maximum temperature at core of the weld pool to the melting point at heat-affected zone and weld metal interface. For calculating melting efficiency, a maximum bulk temperature ($\bar{T} \cong T_{\max}$) is considered. The maximum temperature depends on the electrode polarity. AC square wave welding has an advantage that an electrode remains purely +ve or −ve polarity at a given instance with an almost constant voltage. Therefore, the temperature of a weld pool can be related to EN ratio. If the temperature at extreme EN ratios (0 and 1) could be estimated, values of the maximum bulk temperature at intermediate EN ratios can be expressed using linear interpolation as follows:

$$\frac{\bar{T} - T_1}{T_2 - T_1} = \frac{E - E_1}{E_2 - E_1} \tag{9}$$

where T_1 and T_2 are maximum average temperatures at EN ratios of 0 and 1, respectively (i.e., $E_1 = 0$ and $E_2 = 1$)

$$\bar{T} = T_1 + E(T_2 - T_1) \tag{10}$$

The theoretical bead area for EN = 0 and 1 can be calculated using the fact that, on an average DCEP and DCEN in SAW yield 4% and 8% less material deposited than what is melted at electrode [27], respectively, hence

$$\text{for} \quad \text{DCEP (i.e., EN} = 0)(A_{\text{th}})_P = (A_p)_P + \frac{(A_r)_P}{0.96} \tag{11}$$

$$\text{for} \quad \text{DCEN (i.e., EN} = 1)(A_{\text{th}})_E = (A_p)_E + \frac{(A_r)_E}{0.92} \tag{12}$$

where $(A_{\text{th}})_P$, $(A_p)_P$, and $(A_r)_P$ are the theoretical area, penetration area, and reinforcement area of DCEP polarity and $(A_{\text{th}})_E$, $(A_p)_E$, and $(A_r)_E$ are the theoretical area, penetration area, and reinforcement area of DCEN polarity, respectively.

The theoretical area so calculated can be related to heat input and change in enthalpy (which is a function of the maximum temperature). The maximum temperature can be calculated by inverse computing the corresponding enthalpy as follows:

$$(A_{\text{th}})_{E \text{ or } P} = \frac{\hat{v}\, M_{\text{eq}}}{(H_{T_{\max}} - H_{T_a})} \times H_a \tag{13}$$

$$H_{T_{\max}} = H_{T_a} + \frac{\hat{v}\, M_{\text{eq}}}{A_{\text{th}}} \times H_a \tag{14}$$

where $(A_{\text{th}})_{E \text{ or } P}$ is the theoretical area of either DCEN or DCEP SAW. The maximum temperatures of the investigated material under the process conditions are computed as 2854.7 °C and 2996.7 °C at the EN ratios 0 and 1, respectively.

The heat input per unit length can be calculated from the dynamic current–voltage variation (Fig. 3). If variation in current and voltage is measured every Δt time for n number of intervals, then H_a can be calculated as follows:

$$H_a = \frac{\eta \sum V_a I_a \Delta t}{ns\Delta t} = \frac{\eta \sum V_a I_a}{ns}, \text{J/mm} \tag{15}$$

where V_a and I_a are instantaneous actual voltage and current in Volt and Ampere, respectively, η is arc efficiency, n is number of intervals, and s is welding speed in mm/s.

4 Mathematical Model for Heat Consumption and Melting Efficiency

4.1 Model Development. Calculating heat input and melting efficiency for a given process condition requires a measurement of current–voltage signals and cross-sectional area (a destructive and time-consuming exercise). Once the melting efficiency and heat input are calculated for a wide range of process parameters, they can be presented as a function of such process parameters through statistical modeling. In the present investigation, a second-order polynomial is used to establish a correlation between the input process parameters and responses. The general form of the second-order equation, without considering a constant term, can be written as

$$Y = \sum b_i X_i + \sum b_{ii} X_i^2 + \sum b_{ij} X_i X_j \tag{16}$$

where Y represents responses, X_i, X_j are input process parameters, b_i is the coefficient of the first-order terms, b_{ii} is the coefficient of the second-order terms, and b_{ij} is the coefficient of interaction terms. The values of these coefficients were obtained from MINITAB 2017 STATISTICAL software using stepwise regression model. The heat consumption (HI) and melting efficiency model equations developed using stepwise regression are as follows:

$$\text{HI} = 0.012197\, I - 0.000179\, I.s \tag{17}$$

$$\eta_p = 0.05786\, I - 0.000026\, I^2 - 0.01910\, E.I + 0.001116\, I.s \tag{18}$$

$$\eta_e = 0.08698\, I + 20.76\, E^2 - 0.000055\, I^2 - 0.276\, E.s \tag{19}$$

The efficacy of the proposed models was verified by analysis of variance, as shown in Table 3. The p-value that represents a probability of a null hypothesis (i.e., the model has no effect) approaches zero while other attributes coefficient of correlation (R) and coefficient of determination (R^2) approach 100%. This shows that developed models have a very good capability to understand the parameters and output relation and thereby accurately predict unknown data.

4.2 Model Validation. The average errors in prediction from models for heat input, plate melting efficiency, and electrode melting efficiency are around 10%, 7%, and 6%, respectively,

Table 3 Analysis of variance result of responses

	Regression			Residual			Model features				
Responses	SS	DF	MS	SS	DF	MS	F-value	P-value	R (%)	R^2 (%)	APPE
Heat consumption	262.199	2	131.10	2.169	19	0.114	1148.5	0.00	96.76	99.18	10.18
Plate melting efficiency	34625.9	4	8656.47	178.6	17	10.50	824.2	0.00	94.76	99.49	6.55
Electrode melting efficiency	21034.9	4	5258.73	87.4	17	5.14	1022.8	0.00	84.82	99.59	5.36

SS—sum of squares; DF—degrees-of-freedom; MS—mean square; F—F ratio; R—coefficient of correlation; R^2—coefficient of determination; APPE—average percentage prediction error.

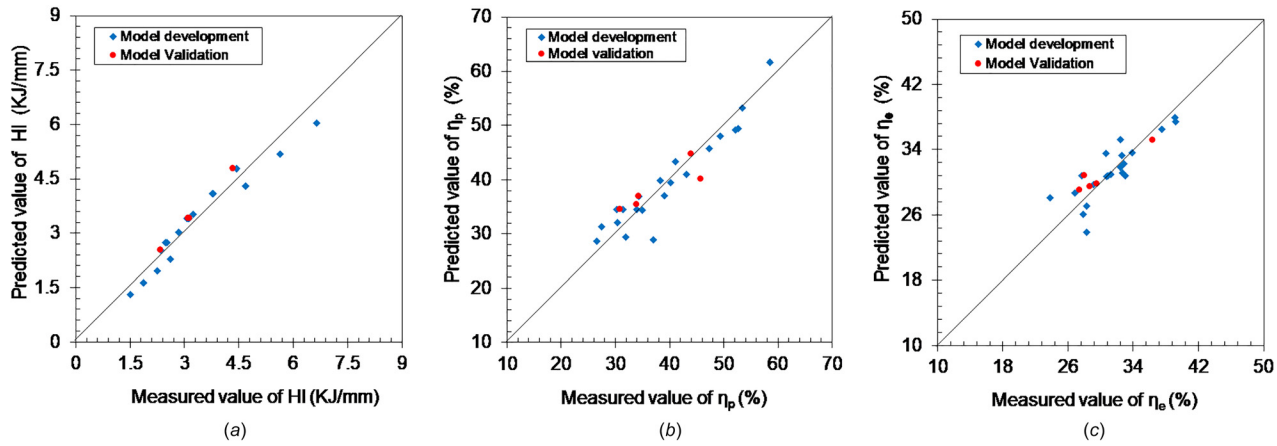

Fig. 7 Prediction of (*a*) heat input, (*b*) plate melting efficiency, and (*c*) electrode melting efficiency

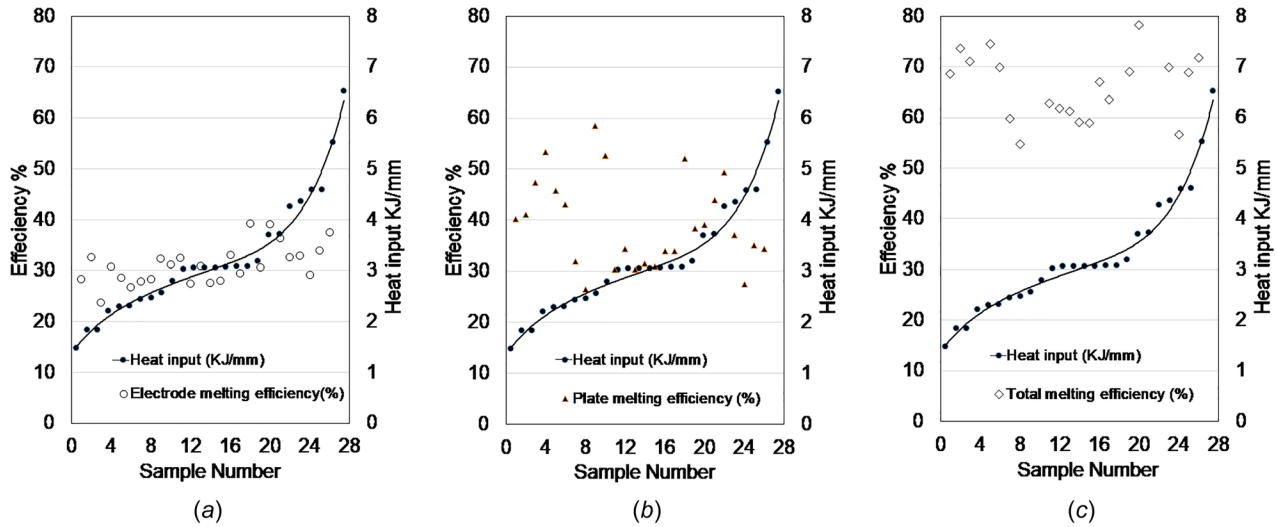

Fig. 8 Relation between heat input and (*a*) plate, (*b*) electrode, and (*c*) total melting efficiency

which shows a good agreement between actual and predicted values. As shown in Table 1, certain experimental runs were kept aside for model validation. The prediction of these data is in very good agreement with the actual data, as shown in Fig. 7.

5 Results and Discussion

5.1 Computation of Melting Efficiency. The computation of melting efficiency requires the maximum temperature of weld metal. The temperature of a weld pool varies from a maximum to the melting point at weld metal heat affected zone interface. The maximum bulk temperatures obtained for DCEP and DCEN are 2854.7 °C and 2996.7 °C, respectively. The bulk, maximum temperature values for EN ratios of 0.25, 0.4, 0.5, and 0.75 are 2890.2 °C, 2911.5 °C, 2925.7 °C, and 2961.2 °C, respectively. For the density value of 0.0079 g/mm^3, the obtained values of the multipliers of H_a in Eq. (4) are 0.0530, 0.0527, 0.0524, and 0.0518, for EN ratios of 0.25, 0.4, 0.5, and 0.75, respectively.

Among the two melting efficiencies, plate melting efficiency varies over a wider range than electrode melting efficiency, as shown in Figs. 8(*a*) and 8(*b*), respectively. Figure 8 maps plate,

electrode, and total melting efficiency against heat input. The increase in heat input due to an increase in welding current improves axial electromagnetic forces with which the droplets knock a weld pool [4]. In turn, the penetration area increases with an increase in heat input, particularly in the range of 1–3 kJ/mm, which helps to improve the plate melting efficiency (Fig. 8(*a*)). Further increase in heat input beyond 3 kJ/mm negatively impacts plate melting efficiency. The increase in heat input per unit length (by a reduction in welding speed) promotes molten metal accumulation beneath the arc, which hinders arc penetration. The individual impact on welding current and speed, along with that of other parameters, are described later.

Unlike plate melting efficiency, electrode melting efficiency remains almost constant with change in heat input (Fig. 8(*b*)). With an increase in heat input induced by an increase in current, melting of plate and electrode proportionately increases, and the ratio of reinforcement area to the total area remains constant, which prevents melting efficiency from considerably changing. Moreover, the proportion of heat used in melting an electrode is less than that for melting a plate. This keeps the melting efficiency numerically small and large variation is not expected. At higher heat input values, the total melting area is dominated by the reinforcement area because of a limited growth of penetration area with an increase in heat, as explained earlier. Therefore, no significant change is observed in melting efficiency at higher heat input values.

5.2 Interplay Between Heat Input and Total Melting Efficiency. The total melting efficiency is a sum of plate and electrode efficiencies. The total melting efficiency inherits distinct patterns of plate melting efficiency and electrode melting efficiency that are quite stable over a wide range of heat input values. The plate melting efficiency, therefore, has a wider range of variation compared to electrode melting efficiency, but less volatility than plate melting efficiency, as shown in Fig. 8(*c*). The gross effect of melting efficiency not only impacts the efficient use of heat but also relates to the consumption of welding flux. The flux consumption (i.e., melting of welding flux and converting into slag) directly affects the weld quality. Too low flux consumption may be a result of having less heat available, i.e., only enough to melt electrode and plate, and results in lack of heat available for flux melting. In such a situation, weld metal is contaminated with unmelted flux and other gaseous substances. Moreover, removal of flux after welding also becomes an issue as slag sticks to weld surface. On the other hand, over-melting of flux may lead to breaking flux cavity and flowing of molten flux. In addition, a thick layer of molten flux may not allow entrapped gases to escape. The utilization of flux is measured in terms of flux-to-wire ratio (FWR), i.e., the weight ratio of flux consumed to deposited metal. FWR is an important factor to assess the quality and productivity of welding procedures. Practical experience suggests that an optimum value of FWR lies between 0.7 and 0.9 [28]. The heat input and total melting efficiencies are not predictably related; however, heat input is a source of melting of metal and flux. Interestingly, the melting efficiency and FWR have a direct relation, as shown in Fig. 9.

The process conditions that yield higher melting efficiencies also result in a reduction of FWR. The benefits are twofold in terms of effective utilization of energy and resources vis-s-vis improved sustainability of the welding process, which has been an important attribute of shop floor-applicable welding processes [29]. The outcome also provides a scenario for multicriteria optimization as melting efficiency cannot be unconditionally increased. The practical range of FWR (0.7–0.9) imposes a limit on melting efficiency that should be pursued; e.g., for the current set of experiments, the limit on FWR restricts the operable range of melting efficiency to around 74–88.5%.

5.3 Effect of Process Variables on Melting Efficiency. The plate melting efficiency is a function of the welding current, welding speed, and EN ratio. The frequency does not impact plate melting efficiency. The droplets impinging on weld pool transfer heat and momentum to the base plate and thereby melt it. The droplet detachment frequency remains very high (of the order of 1000 Hz or more), whereas the current frequency in the investigation is too low. In addition, the current reversal in the square wave is instantaneous. Therefore, a change in frequency does not impact melting of the base plate or plate melting efficiency. The effect of welding current is clearly visible on plate melting efficiency (Fig. 10(*a*)). With an increase in current, the number of molten metal droplets and force with which they act on weld pool enhance melting of plate and plate melting efficiency. The heat input per unit length increases with a reduction in welding speed. As a result, accumulated molten metal hinders arc penetration. Therefore, higher plate melting efficiency is observed at higher speeds (Figs. 10(*a*) and 10(*b*)). The results obtained for change in current and welding speed agree with those of Lee et al. [22] and Chandel [24]. This outcome further establishes the utility of square waveform arc welding as it is known to support weld penetration, even at very high welding speeds [8].

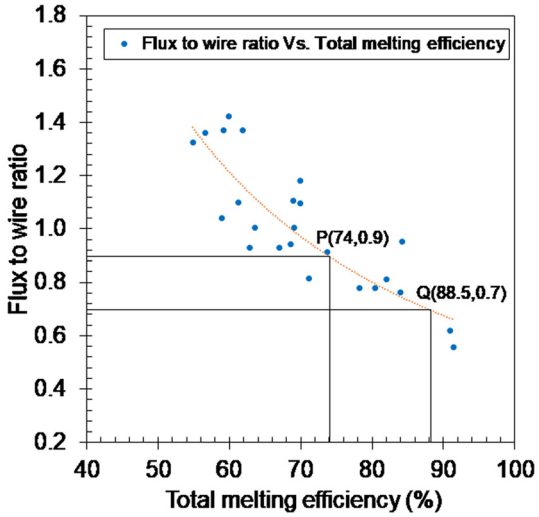

Fig. 9 Relation between flux-to-wire ratio and total melting efficiency

The melting efficiency results can be corroborated by analyzing the effects of process parameters on the melting of electrode (i.e., reinforcement area) and plate melting (i.e., penetration area), as shown in Fig. 11. Figure 11(*a*) shows the effect of welding current (400 A and 700 A, respectively) on the amount of melting of plate and electrode. The extent of increased plate melting can be understood from the right-hand side in Fig. 11(*a*), which shows a higher welding current. An increase in welding speed reduces the overall cross section area, as shown in Fig. 11(*b*) (20 cm/min and 50 cm/min). It can also be seen that the proportion of plate melting is more than electrode melting at higher welding speeds (right-hand side) than at lower welding speeds. Therefore, electrode melting efficiency increases with welding speed. The EN ratio comparison in Fig. 11(*c*) shows that an increase in EN ratio does not change plate melting (penetration area); however, the overall area increases due to increases in electrode melting (reinforcement area). This leads to a marginal change in plate melting efficiency.

The EN ratio also impacts plate melting efficiency. An increase in EN ratio leads to a reduction in plate melting efficiency. When the electrode is negative, positively charged heavy particles hit electrode, whereas, for positive electrodes, light negatively charged particles hit electrode with larger momentum. In the former case, a large amount of molten metal is produced, but droplet temperature is not as high as that recorded with the latter (i.e., positive electrode). Eventually, with an increase in EN ratio, plate melting efficiency decreases.

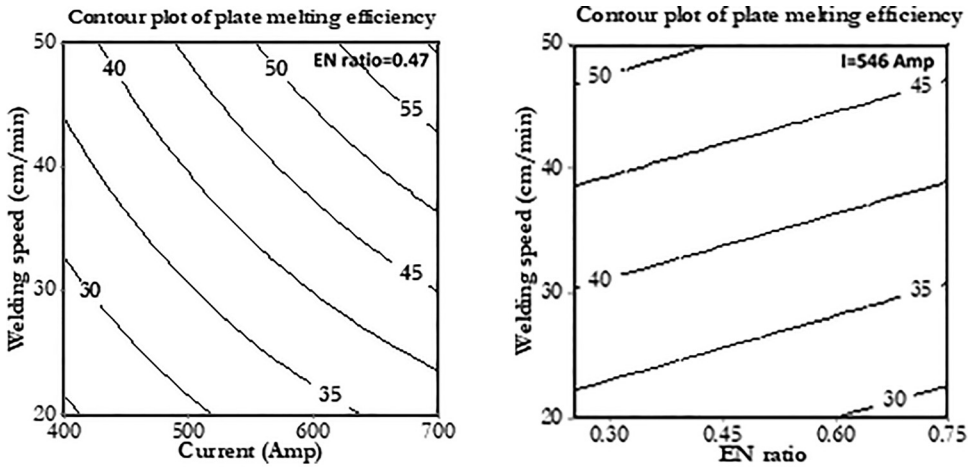

Fig. 10 Effect of process parameters on plate melting efficiency

The electrode melting efficiency primarily depends on welding current and EN ratio. The welding speed is a minor contributor, as can be seen in an almost steep line in the contour plots in Figs. 12(*a*) and 12(*b*). The electrode melting is almost independent of welding speed. The minor impact is due to a disturbance in contact between welding arc plasma and weld pool at higher speed. Therefore, a reduction in melting efficiency can be observed at higher speed (Fig. 12). The welding current impacts electrode's melting by Joule heating and arc heating, which are directly proportional to the square of current and current, respectively. The electrode melting rate is higher at negative polarities because of the reasons explained earlier.

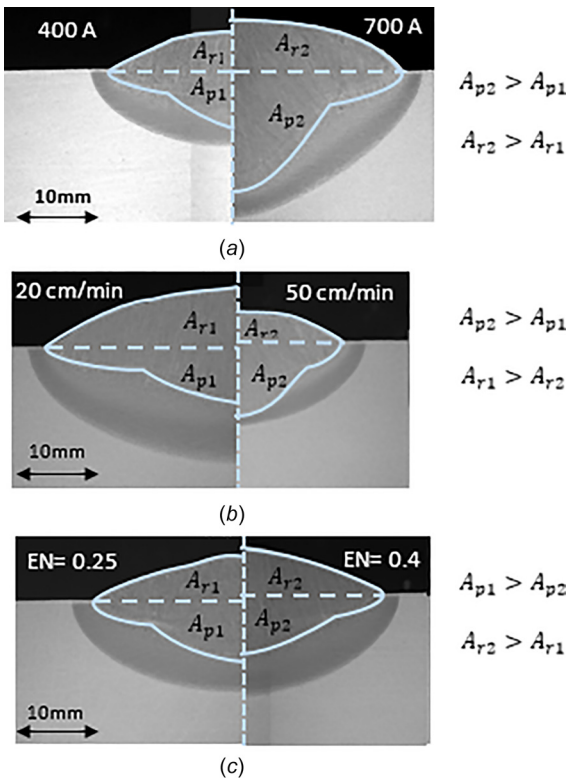

Fig. 11 Effect of process parameters on melting of plate and electrode (*a*), current (*b*), and welding speed (*c*) EN ratio

5.4 Performance Evaluation of Alternating Current Square Waveform Submerged Arc Welding. The performance of AC square waveform SAW is given in Table 4. Within the experimented range of process parameters, AC square waveform SAW can yield a heat input in a range of 1.5 to 6.65 kJ/mm, i.e., AC square waveform weld can match a desired heat input range for the considered material, which is between 2 and 2.5 kJ/mm. The deposition rate of 66–177 g/min is less than that desired at the shop floor. However, AC square waveform is unique in the sense that it maintains penetration even at higher welding speeds. Therefore, loss in deposition rate can be compensated by performing welding at higher currents and higher speeds such that heat input per unit length remains in the expected range (i.e., 2–2.5 kJ/mm). The higher deposition rates of DCEP and DCEN also lead to unusual weld bead shapes with large weld toe angles that form notches at the weld toe.

Efficient use of heat in melting electrode (i.e., electrode melting efficiency) has a direct relation with deposition rate, as shown in Fig. 13—higher the electrode melting efficiency higher the deposition rate. The process conditions that are responsible for an increase in electrode melting efficiency are also responsible for the increase in deposition rate. However, the process conditions that maximize deposition rate can yield plate melting efficiency over a wide range (e.g., 35–55%). This indicates that a proper selection of welding conditions could optimize the deposition rate with near-maximum plate melting efficiency, as shown in the bands in Fig. 13.

The AC square waveform can yield maximum melting efficiency values up to 95%, which is very close to the melting efficiency of DCEP and DCEN under identical conditions. The additional feature of AC square waveform is that it can yield desired flux-to-wire ratio (0.7–0.9), as explained earlier. On the other hand, the DCEP and DCEN lead to undesirable reduction in the flux-to-wire ratio, (0.48–0.49), as shown in Table 4. The AC square waveform is controlled by two additional parameters (frequency and EN ratio), compared to the DC power source. In order to satisfy the requirement of optimality, the additional parameters provide more freedom to fine-tune the process and thereby efficiently use electrical energy.

This work offers new findings on square waveform submerged arc welding in general and for heat-resistant steel welding in particular. It is one of the first investigations that present a method to calculate electrode and plate melting efficiencies in AC square waveform welding and relate them to process parameters via a mathematical function. Quantification of the effect of EN ratio on melting efficiency is one of the most significant contributions among several novel contributions. The distribution of welding

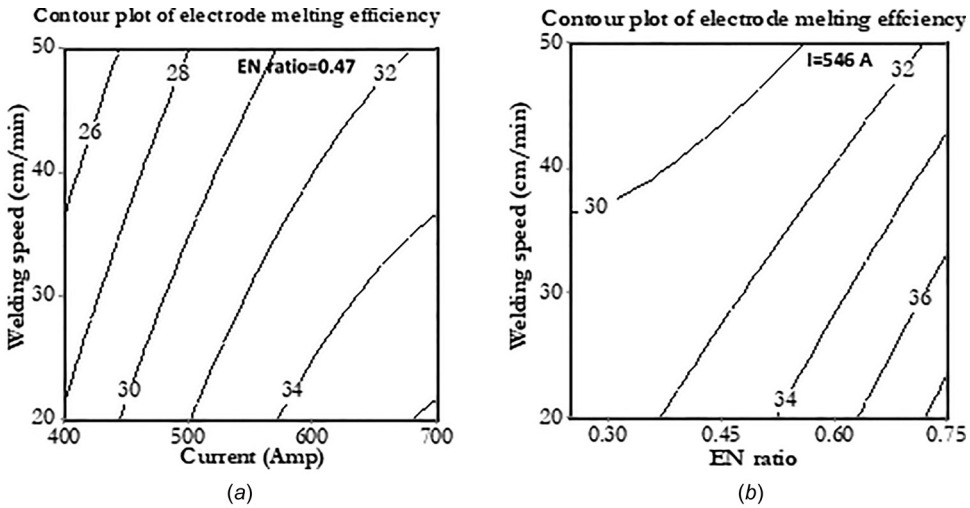

Fig. 12 Effect of process parameters on electrode melting efficiency

Table 4 Capabilities of AC square and comparison with DC SAW

Capabilities of AC square waveform			Comparison of AC square waveform with DC SAW		
AC square			DCEN	DCEP	AC square
Process variables range	Frequency (Hz)	20–80	—	—	60
	EN ratio	0.25–0.75	1	0	0.5
	Current (A)	400–700	500	500	500
	Welding speed (cm/min)	20–50	30	30	30
Range of responses	Heat input (kJ/mm)	1.50–6.65	5.78	5.98	3.11
	Deposition rate (g/min)	66–177	267	261	99
	Flux consumption (g/min)	66.2–147.1	129.15	127.35	135.9
	Flux to wire ratio	0.56–1.43	0.48	0.49	1.37
	Melting efficiency (%)	54.7–95.2	96.37	98.41	59.09
			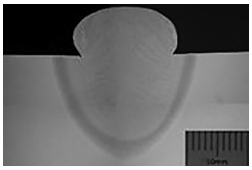	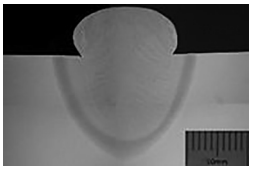	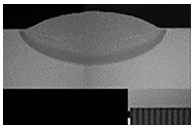

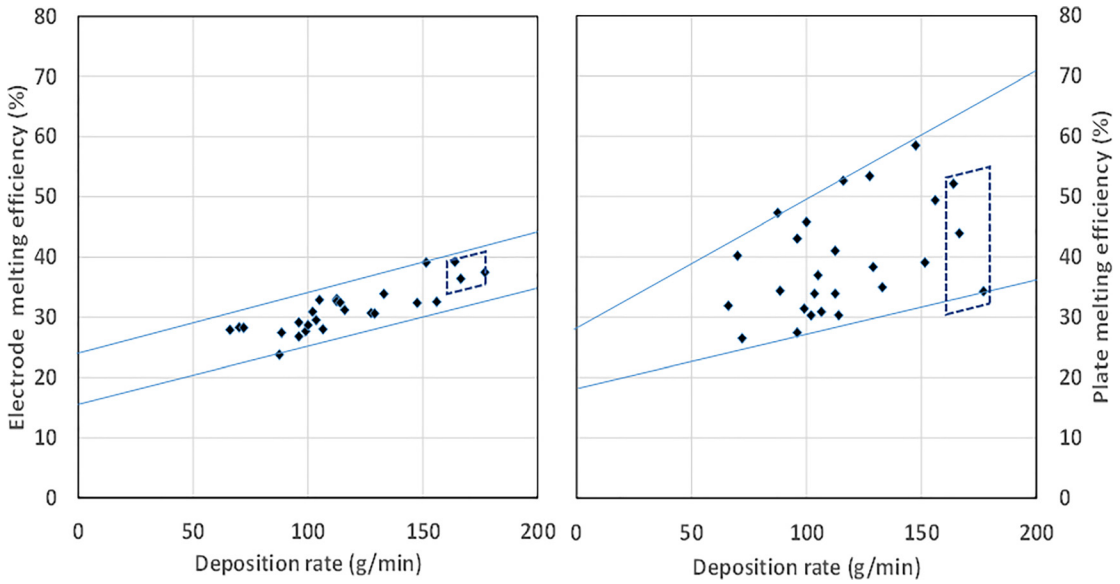

Fig. 13 Relation between deposition rate and melting efficiencies

heat in between plates and electrode and the relationship between welding heat and flux consumption are elucidated by the present investigation. The results of this investigation will provide end-users insight into the AC square process that can help to design a welding procedure for shop-floor applications. This work can be horizontally deployed to other welding processes and materials.

6 Conclusions

The article presents a performance evaluation of AC square waveform power source for submerged arc welding of thick welds by computing melting efficiency and relating it to process conditions and outputs such as deposition rate and flux-to-wire ratio. The following conclusions are drawn from the investigation:

(1) The investigation, one of the first of its kind, shows that plate and electrode melting efficiencies can be calculated via estimation of the volume of metal melted by experimentally measured heat input. The actual heat input, being a predictable function of process parameters, makes it possible to predict plate and electrode melting efficiencies as functions of welding process parameters.
(2) Among the investigated process parameters, welding current and EN ratio most significantly affect melting efficiency in square wave submerged arc welding. The welding speed has a considerable effect on plate melting efficiency but a minor impact on electrode melting efficiency. The current frequency does not affect plate and electrode melting efficiencies. Overall, plate melting efficiency is more sensitive to changes in welding conditions than electrode melting efficiency.
(3) The square waveform facilitates better control of welding due to additional parameters (like EN ratio and frequency) that assist in fine-tuning the process. The AC square waveform outperforms conventionally used DC power sources in terms of judicious use of welding heat.
(4) The deposition rate is directly proportional to electrode melting efficiency, but the same is not true for the plate melting efficiency. A proper selection of welding conditions results in optimal deposition rate (and electrode melting efficiency, as well) with near-maximum plate melting efficiency.
(5) A close relation exists between flux-to-molten metal weight ratio (flux-to-wire ratio) and melting efficiency. For a desirable flux-to-wire ratio of 0.7–0.9, the total melting efficiency can be obtained in a range of 74–88.5%. Overemphasis on melting rate or deposition rate leads to underutilization of welding flux that is detrimental for weld quality.

Acknowledgment

The authors gratefully acknowledge the support provided under a joint project between Hitachi Zosen Corporation, Indian Institute of Technology Hyderabad, India, and Joining and Welding Research Institute, Osaka, Japan (Ja19990018).

Nomenclature

A_i = atomic mass of the element
A_p = penetration area, mm^2
$(A_p)_E$ = penetration area of DCEN polarity, mm^2
$(A_p)_P$ = penetration area of DCEP polarity, mm^2
A_r = reinforcement area, mm^2
$(A_r)_E$ = reinforcement area of DCEN polarity, mm^2
$(A_r)_P$ = reinforcement area of DCEP polarity, mm^2
A_th = theoretical cross-sectional area, mm^2
$(A_\mathrm{th})_E$ = theoretical cross-sectional area of DCEN polarity, mm^2
$(A_\mathrm{th})_P$ = theoretical cross-sectional area of DCEP polarity, mm^2
$(A_\mathrm{th})_{E\,\mathrm{or}\,P}$ = theoretical cross-sectional area of DCEN or DCEP polarity, mm^2
b_i = coefficient of the first-order terms
b_{ii} = coefficient of the second-order terms
b_{ij} = coefficient of interaction terms
C_p = specific heat at constant pressure, J/g K
E = EN ratio
$E_\mathrm{Fusion\,Zone}$ = energy of the fusion zone
E_Loss = energy loss
E_Total = total arc energy
$E_\mathrm{Workpiece}$ = energy of the workpiece
E_1 = EN ratio of DCEP polarity
E_2 = EN ratio of DCEN polarity
H_a = actual heat input, kJ/mm
H_{T_a} = enthalpy at ambient temperature, J/g
H_{T_m} = enthalpy at melting point temperature, J/g
H_{T_max} = enthalpy at maximum temperature, J/g
HI = heat consumption, kJ/mm
I = current, A
I_a = instantaneous actual current, A
M_eq = equivalent molecular weight
n = number of intervals
p_i = percentage contribution
q = heat required to melt weld metal, J
q_eq = heat required to melt a unit mass of metal
s = welding speed, cm/min
T = temperature at any instant, K
T_m = melting temperature, K
T_max = maximum temperature, K
T_1 = temperature at EN ratio 0, K
T_2 = temperature at EN ratio 1, K
$\hat{v}$ = specific volume of weld metal, mm^3/g
V_a = instantaneous actual voltage, V
X_i, X_j = input parameters
Y = responses
α = constant to enter or remove number of terms
ΔH_{T_m} = enthalpy difference between the melting point temperature and ambient temperature, J/g
η = arc efficiency
η_e = electrode melting efficiency
η_m = total melting efficiency
η_p = plate melting efficiency

References

[1] Zhenglong, L., Caiwang, T., Yanbin, C., and Zhongshao, S., 2013, "Microstructure and Mechanical Properties of Fiber Laser-Metal Active Gas Hybrid Weld of X80 Pipeline Steel," ASME J. Pressure Vessel Technol., **135**(1), p. 011403.
[2] Tan, J., Huang, W., and Chao, Y. J., 2006, "Prediction of Fracture Appearance Transition Temperature of 2.25 Cr-1Mo Steel Used in Hot-Wall Hydrofining Reactors," ASME J. Pressure Vessel Technol., **128**(4), pp. 566–571.
[3] Yu, E., Han, Y., Xiao, H., and Gao, Y., 2017, "Numerical Analysis of Microstructure and Residual Stress in the Weld Zone of Multiwire Submerged Arc Welding," ASME J. Pressure Vessel Technol., **139**(2), p. 021404.
[4] Sharma, A., Arora, N., and Mishra, B. K., 2008, "A Practical Approach Towards Mathematical Modeling of Deposition Rate During Twin-Wire Submerged Arc Welding," Int. J. Adv. Manuf. Technol., **36**(5–6), pp. 463–474.
[5] Pedrazzo, G., Barone, C. A., and Rutili, G., 2009, "AC/DC Generators With Waveform Control: Innovation in Submerged Arc Welding," Weld. Int., **23**(11), pp. 839–845.
[6] Toma, R. E., Brandi, S. D., Souza, A. C., and Morais, Z., 2011, "Comparison Between DC (+) and Square Wave AC SAW Current Outputs to Weld AISI 304 for Low-Temperature Applications," Weld. J., **90**(9), pp. 153S–160S.
[7] Cho, D. W., Song, W. H., Cho, M. H., and Na, S. J., 2013, "Analysis of Submerged Arc Welding Process by Three-Dimensional Computational Fluid Dynamics Simulations," J. Mater. Process. Technol., **213**(12), pp. 2278–2291.
[8] Mohanty, U. K., Sharma, A., Nakatani, M., Kitagawa, A., Tanaka, M., and Suga, T., 2018, "A Semi-Analytical Nonlinear Regression Approach for Weld Profile Prediction: A Case of Alternating Current Square Waveform Submerged Arc Welding of Heat Resistant Steel," ASME J. Manuf. Sci. Eng., **140**(11), p. 111013.
[9] Mendez, P. F., Goett, G., and Guest, S. D., 2015, "High-Speed Video of Metal Transfer in Submerged Arc Welding," Weld. J., **94**(10), pp. 325 s–332 s.
[10] Pepin, J., 2009, "Effects of Submerged Arc Weld (SAW) Parameters on Bead Geometry and Notch-Toughness for X70 and X80 Linepipe Steels," Ph.D. dissertation, University of Alberta, Edmonton, AB, Canada.

[11] Su, Y., Hua, X., and Wu, Y., 2013, "Effect of Input Current Modes on Intermetallic Layer and Mechanical Property of Aluminum–Steel Lap Joint Obtained by Gas Metal Arc Welding," Mater. Sci. Eng., A, **578**, pp. 340–345.
[12] Kah, P., Salminen, A., and Martikainen, J., 2010, "The Effect of the Relative Location of Laser Beam With Arc in Different Hybrid Welding Processes," Mechanics, **83**(3), pp. 68–74.
[13] Bajcer, B., Hrženjak, M., Pompe, K., and Jež, B., 2006, "Improvement of Energy and Materials Efficiencies by Introducing Multiple-Wire Welding," Metalurgija, **46**(1), pp. 47–52.
[14] Unocic, R. R., and DuPont, J. N., 2004, "Process Efficiency Measurements in the Laser Engineered Net Shaping Process," Metall. Mater. Trans. B, **35**(1), pp. 143–152.
[15] Shen, S., Oguocha, I. N. A., and Yannacopoulos, S., 2012, "Effect of Heat Input on Weld Bead Geometry of Submerged Arc Welded ASTM A709 Grade 50 Steel Joints," J. Mater. Process. Technol., **212**(1), pp. 286–294.
[16] Rodrigues, A., and Loureiro, A., 2005, "Effect of Shielding Gas and Activating Flux on Weld Bead Geometry in Tungsten Inert Gas Welding of Austenitic Stainless Steels," Sci. Technol. Weld. Joining, **10**(6), pp. 760–765.
[17] Park, Y. D., Kang, N., Malene, S. H., and Olson, D. L., 2007, "Effect of Exothermic Additions on Heat Generation and Arc Process Efficiency in Flux-Cored Arc Welding," Met. Mater. Int., **13**(6), pp. 501–509.
[18] Tušek, J., and Suban, M., 2003, "High-Productivity Multiple-Wire Submerged-Arc Welding and Cladding With Metal-Powder Addition," J. Mater. Process. Technol., **133**(1–2), pp. 207–213.
[19] Salminen, A. S., 2003, "Effects of Filler Wire Feed on the Efficiency of Laser Welding," First International Symposium on High-Power Laser Macroprocessing, International Society for Optics and Photonics, Osaka, Japan, Vol. 4831, pp. 263–269.
[20] Zhu, S., Wang, Q. W., Wang, X. M., and Han, G. F., 2011, "Analysis on Thermal Efficiency and Softening Behavior of MIG Welding With Longitudinal Magnetic Field," Adv. Mater. Res., **148**, pp. 326–331.
[21] Walsh, C. A., Bhadeshia, H. K. D. H., Lau, A., Matthias, B., Oesterlein, R., and Drechsel, J., 2003, "Characteristics of High-Power Diode–Laser Welds for Industrial Assembly," J. Laser Appl., **15**(2), pp. 68–76.
[22] Lee, C. S., Chandel, R. S., and Seow, H. P., 2000, "Effect of Welding Parameters on the Size of Heat Affected Zone of Submerged Arc Welding," Mater. Manuf. Processes, **15**(5), pp. 649–666.
[23] Achebo, J. I., and Oghoore, O., 2012, "Numerical Computation of Melting Efficiency of Aluminum Alloy 5083 During CO_2 Laser Welding Process," *Materials With Complex Behaviour II*, Springer, Berlin, pp. 601–617.
[24] Chandel, R. S., 1990, "Electrode Melting and Plate Melting Efficiencies of Submerged Arc Welding and Gas Metal Arc Welding," Mater. Sci. Technol., **6**(8), pp. 772–777.
[25] Niles, R. W., and Jackson, C. E., 1975, "Weld Thermal Efficiency of the GTAW Process," Weld. J., **54**(1), p. 25.
[26] King, B., 2005, "Welding and Post Weld Heat Treatment of 2.25% Cr-1% Mo Steel," Master thesis, Faculty of Engineering, University of Wollonggong, Wollongong, Australia, pp. 9–40.
[27] Dahiwale, N. B., Kapil, A., and Sharma, A., 2015, "Integrated Model for Assessment of Electromagnetic Force Field Due to Arc Welding," Sci. Technol. Weld. Joining, **20**(7), pp. 563–570.
[28] Campbell, F. C., ed., 2011, Joining: *Understanding the Basics*, ASM International, Materials Park, Novelty, OH.
[29] Sharma, A., 2018, "A Fundamental Study on Qualitatively Viable Sustainable Welding Process Maps," J. Manuf. Syst., **46**, pp. 221–230